J Physiol 590.15 (2012) pp 3449–3464

The Journal of Physiology

Disease-causing mutations C277R and C277Y modify gating of human ClC-1 chloride channels in myotonia congenita

Sebastian Weinberger[1], Daniel Wojciechowski[1], Damien Sternberg[2], Frank Lehmann-Horn[3], Karin Jurkat-Rott[3], Toni Becher[1], Birgit Begemann[1], Christoph Fahlke[1] and Martin Fischer[1]

[1]*Institut für Neurophysiologie, Medizinische Hochschule Hannover, Hannover, Germany*
[2]*Hôpital Pitié-Salpêtrière, Assistance Publique Hôpitaux de Paris, Paris, France*
[3]*Division of Neurophysiology, Universität Ulm, Ulm, Germany*

Key points

- ClC channels are double-barrelled channels with two ion conduction pathways per individual channel.
- Substituting cysteine 277 by serine constitutively opens the common gate suggesting that this residue plays a major role in joint openings/closings of both protopores of ClC-1.
- We studied here the functional consequences of two novel myotonia-associated mutations, C277R and C277Y, of human ClC-1 chloride channels.
- C277Y not only modified the common gate, but also protopore gating.
- C277Y inverts the voltage dependence and reduces the open probabilities of protopore and common gates and thus decreases the absolute open probabilities of homodimeric hClC-1 channels to values below 3%.
- C277Y reduces single protopore current amplitudes to about two-thirds of wild-type values, and inverts the anion permeability sequence.
- Our results explain the disease-causing effects and provide novel insights into the molecular processes underlying normal and pathologically altered function of muscle chloride channels.

Abstract Myotonia congenita is a genetic condition that is caused by mutations in the muscle chloride channel gene *CLCN1* and characterized by delayed muscle relaxation and muscle stiffness. We here investigate the functional consequences of two novel disease-causing missense mutations, C277R and C277Y, using heterologous expression in HEK293T cells and patch clamp recording. Both mutations reduce macroscopic anion currents in transfected cells. Since hClC-1 is a double-barrelled anion channel, this reduction in current amplitude might be caused by altered gating of individual protopores or of joint openings and closing of both protopores. We used non-stationary noise analysis and single channel recordings to separate the mutants' effects on individual and common gating processes. We found that C277Y inverts the voltage dependence and reduces the open probabilities of protopore and common gates resulting in decreases of absolute open probabilities of homodimeric channels to values below 3%. In heterodimeric channels, C277R and C277Y also reduce open probabilities and shift the common gate activation curve towards positive potentials. Moreover, C277Y modifies pore properties of hClC-1. It reduces single protopore current amplitudes to about two-thirds of wild-type values, and inverts the anion permeability sequence to $I^- = NO_3^- > Br^- > Cl^-$. Our findings predict a dramatic reduction of the muscle fibre resting chloride conductance and thus fully explain the disease-causing effects

DOI: 10.1113/jphysiol.2012.232785

of mutations C277R and C277Y. Moreover, they provide additional insights into the function of C277, a residue recently implicated in common gating of ClC channels.

(Received 27 March 2012; accepted after revision 25 May 2012; first published online 28 May 2012)
Corresponding author M. Fischer: Institut für Neurophysiologie, Medizinische Hochschule Hannover, Carl-Neuberg-Str. 1, 30625 Hannover, Germany. Email: fischer.martin@mh-hannover.de

Abbreviations hClC-1, human muscle chloride channel; HEK293T, human embryonic kidney cells expressing the SV40 large T-antigen; WT, wild-type; YFP, yellow fluorescent protein.

Introduction

Myotonia congenita is an inherited human disease characterized by delayed muscle relaxation and muscle stiffness following forceful contractions. Autosomal dominant myotonia congenita (Thomsen's disease) and autosomal recessive generalized myotonia (Becker's myotonia) are caused by mutations in the major skeletal muscle chloride channel gene (*CLCN1*) (Koch *et al.* 1992; George *et al.* 1993). So far, more than 100 mutations of *CLCN1* have been identified in patients with myotonia congenita. Analysis of the functional consequences of certain myotonia-associated mutations not only provided important insights into the physiological impact of hClC-1 channel gating and permeation but also in mechanisms and molecular determinants of these processes (Fahlke *et al.* 1995, 1997*a*; Wollnik *et al.* 1997; Saviane *et al.* 1999).

hClC-1 belongs to the ClC family of anion channels (ClC-0, ClC-1, ClC-2 and ClC-Ka/Kb) and anion/proton antiporters (ClC-3–ClC-7) (Jentsch, 2008). All ClC proteins are dimers, and each subunit exhibits an individual ion permeation pathway (Dutzler *et al.* 2002; Feng *et al.* 2010). This architecture results in two largely independent protopores of ClC channels that are opened and closed by two structurally distinct gating processes (Miller, 1982). For all ClC channels studied so far, fast gating opens and closes individual protopores, whereas slow cooperative gating steps act simultaneously on both protopores (Miller, 1982; Saviane *et al.* 1999; Zuniga *et al.* 2004; de Santiago *et al.* 2005; Fischer *et al.* 2010).

A common gate of ClC channels has not yet been defined at the structural level and simultaneous opening and closing transitions are most likely mediated by cooperative interactions between the two protopores. Mutations of certain amino acids in the interface region between ClC monomers were reported to alter the open probability of the common gate of hClC-1 (Duffield *et al.* 2003). For hClC-1 as well as the prototypic ClC channel ClC-0 from *Torpedo marmorata*, exchanging a conserved cysteine at the end of the G helix to serine locks the slow gate in a constitutively open state (Lin *et al.* 1999; Accardi & Pusch, 2000; Zuniga *et al.* 2004; de Santiago *et al.* 2005). We studied here the functional consequences of two naturally occurring disease-causing mutations that predict substitution of this cysteine residue by arginine or tyrosine (C277R or C277Y) on the human muscle chloride channel hClC-1. We observed markedly reduced chloride conductance as a consequence of changes in both the fast and the slow gating process. A detailed analysis of one of the studied mutations, C277Y, further revealed altered pore properties and elucidated new aspects of gating in hClC-1.

Parts of this study were reported as an abstract (Weinberger *et al.* 2011).

Methods

Clinical data

Patient 1 was a 23-year-old man, with five healthy siblings, non-consanguineous healthy parents and no other case history reported in the family. Myotonic symptoms were noticed from age 11. Muscle stiffness was apparent at the beginning of movements, but resolved upon repetitive movements with slight aggravation under cold conditions. The clinical symptoms remained stable over years. EMG examination showed myotonic discharges in all muscles with numerous typical myotonic bursts triggered by muscle contraction, muscle percussion or needle mobilization.

Patient 2 was a 22-year-old man, with no other affected family member. He was referred with a diagnosis of Becker's myotonia congenita. The age of onset of symptoms was not precisely known. Myotonia was confirmed by EMG.

Patient 3 was another 22-year-old man with two affected sisters, one healthy brother and non-consanguineous healthy parents. Disease was first noticed at age 7. Muscle stiffness and contracture were present at the onset of physical efforts with additional sensation of blockade and weakness that disappeared with maintained physical activity. There was no aggravation under cold conditions. Musculature was eutrophic, with neither atrophy nor hypertrophy. EMG confirmed the existence of myotonic bursts.

Patient 4 was a 44-year-old woman with one affected brother, four other healthy siblings and consanguineous healthy parents. Clinical symptoms appeared in childhood and consisted of isolated myotonia at onset of effort, which improved with warm-up upon ongoing activity.

EMG showed myotonic bursts. Repeated short effort test at ambient temperature and cold showed a type II profile according to classification by Fournier (Fournier *et al.* 2006).

Patient 5 was a 59-year-old man who presented with generalized myotonia and frequent myotonic bursts in EMG. Slight atrophy and weakness of distal forearm muscles were noticed, which may occur in some older myotonia patients and also in the majority of myotonic dystrophy patients. We therefore analysed length of *DMPK* CTG repeats on both alleles and found values within the normal range, excluding myotonic dystrophy in this patient.

DNA sequencing and mutations in *CLCN1*

Genomic DNA was extracted from white blood cells. All 23 *CLCN1* exons and juxta-exonic intronic regions were PCR-amplified as described previously (Lehmann-Horn *et al.* 1995; Bernard *et al.* 2008). All PCR products were bi-directionally sequenced. In patients 1 to 4, we identified a novel *CLCN1* mutation, c.829 T>C p.Cys277Arg (C277R), which predicts the replacement of cysteine 277 by arginine and is located in exon 7. In patient 5, another point mutation in the same codon 277, c.830 G>A p.Cys277Tyr (C277Y), was found. For this patient we performed multiplex ligation-dependent probe amplification (MLPA) analysis for all 23 exons to exclude a copy number variation and thereby to increase the evidence for compound heterozygosity, as recently described (Lehmann-Horn *et al.* 2011). Patients 1 to 3 were heterozygous for the C277R mutation, and had another heterozygous c.501 C>G p.Phe167Leu (F167L) mutation (Zhang *et al.* 2000*a*) on the other allele, thus sharing the same *CLCN1* genotype. Patient 4 was homozygous for the C277R mutation, which was consistent with the parental consanguinity. The parents of patients 1–4 all originated from the Maghreb, thus suggesting a North African founder effect. The family of patient 5 was from Turkey. He was heterozygous for the C277Y mutation, and the evaluation of the remaining sequences revealed another previously unreported missense mutation in exon 14 in a heterozygous state, c.1580 T>C p.Ile527Thr (I527T). All those point mutations were not reported in databases or literature (except for F167L) nor found when resequencing more than 400 control alleles in our laboratories.

The molecular genetics diagnosis for patients 1–4 was performed according to French law, after patients were informed about the nature and diagnostic aim of genetic tests and gave their consent to it. Patient 5 also gave his informed consent, the genetic test procedure being approved of by the Ethics Committee of Ulm University. The studies were in concordance with the *Declaration of Helsinki*.

Mutagenesis and expression of wild-type (WT) and mutant channels

Point mutations were introduced into the plasmid pSVL-hClC-1 containing the full length WT hClC-1 cDNA (Hebeisen & Fahlke, 2005) using the QuikChange site-directed mutagenesis kit (Stratagene, La Jolla, CA, USA). Construction of concatamers was performed as described previously (Fahlke *et al.* 1997*c*). Since there is ample evidence that the order of subunits does not affect the function of concatenated heterodimeric hClC-1 channels (Fahlke *et al.* 1997*c*) concatamers only were generated in the mutant-WT order.

For all constructs, amplified sequences were verified by direct sequencing and two independent mutant clones were used for expression studies. Mutant and WT hClC-1 channels were transiently expressed in HEK293T cells and examined typically 2 days after transfection with a calcium phosphate precipitation method (Fahlke *et al.* 1997*a*). To identify cells with a high probability of expressing recombinant ion channels, cells were co-transfected with a plasmid encoding the CD8 antigen and incubated 5 min prior to use with polystyrene microbeads precoated with anti-CD8 antibodies (Dynabeads M-450 CD 8, Dynal, Great Neck, NY, USA). Current amplitudes were much smaller in cells expressing mutant channels than for WT hClC-1. For electrophysiological recordings we therefore increased the transfected DNA amount from 0.5 μg for WT to 2.7–3.5 μg per dish for mutant channels (10 ml final volume containing about 5 million cells).

To study the effects of C277R and C277Y on expression levels HEK293T cells were transfected with equal amounts of WT or mutant pSVL-YFP-hClC-1 (Hebeisen *et al.* 2004). Cells were lysed 2 days after transfection by incubation in 1% Triton X-100 in the presence of protease inhibitors (Sigma-Aldrich, Hamburg, Germany). Cleared lysates were denatured for 15 min at room temperature in SDS sample buffer containing 100 mM dithiothreitol and electrophoresed in parallel with fluorescence mass markers (Dual Colour; Bio-Rad, München, Germany) on 12% SDS polyacrylamide gels. Proteins were visualized by scanning the wet PAGE gels with a fluorescence scanner (Typhoon; GE Healthcare, München, Germany). Individual bands were quantified with the ImageQuant software (GE Healthcare, Freiburg, Germany).

Electrophysiology

Whole-cell patch clamp recordings were performed as previously described (Hebeisen *et al.* 2003; Hebeisen & Fahlke, 2005). The standard extracellular solution contained (in mM): NaCl (140), KCl (4), $CaCl_2$ (2), $MgCl_2$ (1), Hepes (5), pH 7.4. Bathing solutions with low pH (6.4 and 5.9) were buffered using Mes instead of Hepes. Agar bridges were used to connect the amplifier and the bath solution.

The standard intracellular solution contained (in mM): NaCl (120), $MgCl_2$ (2), EGTA (5), Hepes (10), pH 7.4. Sodium glutamate substituted for NaCl in experiments with low intracellular chloride concentration. NaCl was partially replaced by NaBr, NaI or $NaNO_3$ to study the anion selectivity of hClC-1. Reversal potentials were either determined from current-voltage relationship or by recording the membrane potential with zero current in the current clamp mode three min after cell penetration. Both procedures provided identical results. Relative permeabilities P_X/P_{Cl} were calculated from reversal potentials using the Goldmann–Hodgkin–Katz equation. Results were corrected for junction potentials calculated using the JPCalc software (Dr P. Barry, University of New South Wales, Sydney, Australia; Barry, 1994). Cells were clamped to 0 mV between two test sweeps.

Single channel recordings were performed in the excised inside-out mode. The internal (bath) and external (pipette) solution contained (in mM): NMDG-Cl (130), $CaCl_2$ (2), $MgCl_2$ (5). Solutions were buffered using 10 mM Hepes (pH 7.4) or Mes (pH 6.4). Pipettes were pulled from borosilicate glass and had resistances between 10 and 30 MΩ. Pipette tips were coated with Sigmacote (Sigma-Aldrich Chemie, München, Germany) to reduce their capacitance. Single channels data was acquired with a 1 kHz Bessel filter and subsequently digitally low-pass-filtered at 300 Hz. The occurrence of two equidistant conductance levels that are interrupted by a common closed state is characteristic for double-barrelled ClC channels. We used this criterion and the voltage-dependent rectification and open probability to identify hClC-1. Most patches displayed multi-channel activity, since hClC-1 channels appeared to cluster in the cell membrane. Reliable analysis was restricted to 5 out of 196 patches from cells expressing WT hClC-1 and 7 out of 39 patches from cells expressing C277Y hClC-1.

Data analysis

Data were analysed by a combination of Clampfit (Axon Instruments, Union City, CA) and SigmaPlot (Systat Software Inc., San Jose, CA, USA) programs. Instantaneous current amplitudes were calculated by extrapolating the time course of current traces with mono- or bi-exponential functions to the moment of the voltage step or were measured immediately after capacitive current relaxation ($<500\,\mu$s after the voltage step). Late current amplitudes were obtained at the end of 300 ms pulses of varying potentials. To determine the time course of macroscopic current activation and deactivation, the sum of a mono-exponential or bi-exponential function and a time-independent value ($I(t) = a_1\exp(-t/\tau_{fast}) + a_2\exp(-t/\tau_{slow}) + c$) was fitted to data recorded during a series of voltage steps from a holding potential of 0 mV. To obtain the relative probabilities of channel openings, instantaneous current amplitudes after stepping to –125 mV were plotted *versus* the voltage of a preceding 300 ms pulse and fitted with a modified Boltzmann equation exhibiting a voltage-independent minimum open probability (P_{min}) and a voltage-dependent term: $P(V) = (P_{max} - P_{min})/(1 + e^{z\delta F(V-V0.5)/RT}) + P_{min}$, with $z\delta$ being the apparent gating charge, P_{max} the maximum open probability and $V_{0.5}$ the midpoint of activation.

Single-channel current amplitudes were determined from all-points amplitude histograms that were fit by Gaussian distributions. The relative areas of the different Gaussian components were used to estimate absolute open probabilities.

All values are given as means ± SEM.

Noise analysis

Non-stationary noise-analysis was performed as previously described (Hebeisen & Fahlke, 2005). Currents were filtered at 10 kHz and digitized with a sampling rate of 50 kHz. A series of 50–300 records was recorded by pulsing to a certain voltage and pairs of subsequent records were then subtracted using the *Analysis* software (kindly provided by Dr F. Bezanilla, University of Chicago, USA) to compute the experimental non-stationary ensemble variance (Heinemann & Conti, 1992). Background variance was measured at the reversal potential (−5 mV) and subtracted from current variance. The variance points were sorted into evenly spaced current bins and the statistical errors caused by averaging were superimposed as error bars. Modified non-stationary noise analysis was used to investigate concatamer C277Y-WT hClC-1 exhibiting very slow time course of activation at positive potentials. Here we obtained current variance values from short time bins (2–10 ms) of single current traces (2–5 s) after voltage steps from –5 mV to varying positive potentials.

Results

Functional characterization of C277R and C277Y hClC-1 channels

Cysteine 277 is conserved within ClC-0, ClC-1 and ClC-2 of diverse species, but not in ClC-K channels or ClC Cl^-/H^+-exchangers (Fig. 1*A*). It is located at the carboxy-terminal end of the G helix of hClC-1 in close proximity to the gating glutamate at the end of helix F that marks the entrance of the chloride conduction pathway (Fig. 1*B*). Helix G is also flanked by helices H and I that belong to the interface region between the subunits of hClC-1 (Cederholm *et al.*

2010; Dutzler *et al.* 2002; Duffield *et al.* 2003). Figure 2 shows representative whole-cell recordings from HEK293T cells expressing WT, C277R or C277Y hClC-1 homodimers. Cells were held at 0 mV and voltage steps between −155 mV and +125 mV were applied. WT currents rose instantaneously upon voltage steps in hyper- or depolarizing directions. The instantaneous rise was followed by a bi-exponential deactivation at negative voltages, whereas current amplitudes were time independent at positive potentials (Fig. 2*A*). C277R or C277Y reduced macroscopic current amplitudes so that five- to sixfold increased plasmid DNA amounts were necessary to obtain current amplitudes comparable to WT hClC-1. To test possible consequences of the mutations on protein expression levels, WT and mutant hClC-1 were expressed as yellow fluorescent protein (YFP) fusion protein and quantified as amount of fluorescent proteins after cell lysis and gel electrophoresis (Suppl. Fig. 1). We observed similar expression levels in cells transfected with WT or mutant channel plasmid DNA.

Both mutations exerted pronounced effects on voltage-dependent gating. C277R and C277Y hClC-1 currents activated upon negative as well as upon positive voltage steps (Fig. 2*B* and *C*). Time course of current activation at hyperpolarizing potentials could be well fitted with a single exponential function for C277R ($\tau = 3.5 \pm 0.3$ ms at −155 mV; $n = 8$) but required two exponentials for C277Y hClC-1 ($\tau_{fast} = 9.1 \pm 0.9$ ms and $\tau_{slow} = 110 \pm 15$ ms at −155 mV; $n = 5$). Figure 2*D–F* shows voltage dependences of instantaneous (broken lines) and late current amplitudes (symbols), the latter being obtained at the end of 300 millisecond voltage steps to positive and negative potentials (arrows in Fig. 2*A–C*). Mutant channels differed from WT in instantaneous as well as in late current amplitudes.

C277R and C277Y hClC-1 gating depends on intracellular chloride concentration

ClC channel gating is well known to be modified by the concentrations of permeant anions (Jentsch, 2008). In the past, various myotonia-causing mutations have been shown to exert functional alterations that were distinct at physiologically low and at standard internal anion concentrations (Fahlke *et al.* 1995; Wu *et al.* 2002). We thus investigated WT and mutant channel properties also under a physiological intracellular chloride concentration (4 mM) (Fig. 3). In these experiments, voltage steps were applied from a holding potential of −85 mV close to the calculated reversal potential to prevent voltage-dependent redistribution of Cl^-. Gating of WT hClC-1 was only marginally affected by low internal [Cl^-] as described previously (Hebeisen & Fahlke, 2005). Under these conditions WT channels responded to hyperpolarizing voltage steps with an instantaneous rise in current amplitude followed by bi-exponential current relaxations (Fig. 3*A*), and depolarizing voltage steps induced channel activation after an instantaneous current rise. In both types of mutant channel, reduced internal [Cl^-] abolished hyperpolarization-induced gating (Fig. 3*B* and *C*) so that C277R and C277Y hClC-1 exclusively activated upon depolarization. We conclude that activation of C277R and C277Y hClC-1 by membrane hyperpolarization is markedly dependent on intracellular chloride concentration as reported for other myotonia-associated mutations (Fahlke *et al.* 1995; Zhang *et al.* 2000). The asymmetric anion distribution and exclusive depolarization-induced activation produced C277R and C277Y hClC-1 currents with strong outward rectification (Fig. 3*E* and *F*) and very low macroscopic chloride conductance at resting membrane potentials.

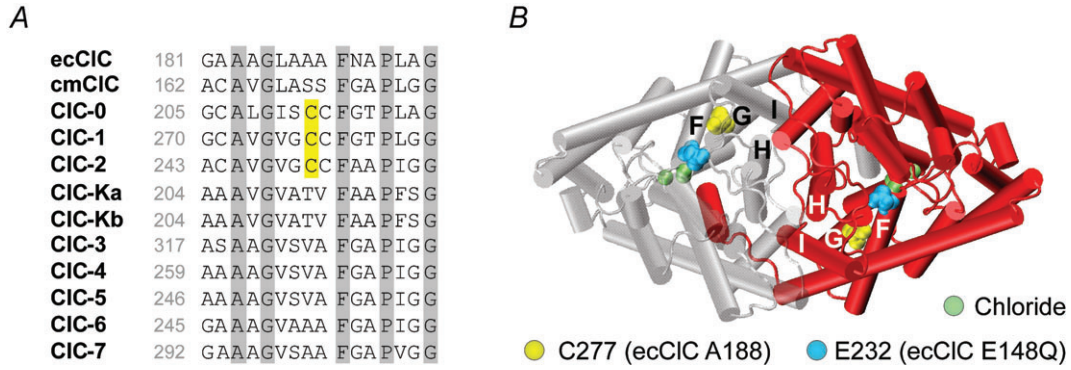

Figure 1. Localization of cysteine 277
A, alignment of the amino acid sequence of different ClC proteins. Cysteine 277 is conserved within ClC-0, ClC-1 and ClC-2, but not in ClC-K channels or human ClC Cl^-/H^+-exchangers (ClC-3 through ClC-7) and their homologues in *E. coli* (ecClC) and the red alga *Cyanidioschyzon merolae* (cmClC). *B*, backbone fold of the bacterial ClC transporter ecClC (Dutzler *et al.* 2002) viewed from the extracellular side of the cell membrane. Side-chain of A188 (homologous to cysteine 277 in hClC-1) is shown in yellow. Green beads represent chloride ions attached to three binding sites within each protopore where the 'gating glutamate' E148 (homologous to E232 in hClC-1) is displayed in the open configuration of the E148Q mutant (coloured in blue).

Functional properties of heterodimeric channels

Skeletal muscle chloride channels are dimers (Fahlke *et al.* 1997*c*), and – in heterozygous patients – homodimeric WT and mutant channels as well as heterodimeric channels harbouring one mutant and one WT subunit co-exist in the sarcolemma. To test for the functional consequences of the disease-causing mutations in heterozygous patients, we first co-transfected cells with equal amounts of WT and mutant hClC-1 (Suppl. Fig. 2). Cells co-expressing WT and C277R hClC-1 display voltage-dependent whole-cell currents that resemble WT currents (Suppl. Fig. 2) indicating that currents conducted by WT homodimers dominate macroscopic current. Upon cotransfection of WT and C277Y, hClC-1 currents displayed time and voltage dependences that differed from WT as well as from mutant currents and could not be interpreted as simple addition of both types of current responses (Suppl. Fig. 2).

To study a homogeneous population of heterodimeric channels we transfected concatameric constructs that link one mutant and one WT sequence in a single open reading frame. Figure 4 shows representative recordings from C277R-WT or C277Y-WT heterodimers under standard recording conditions. C277R-WT currents resembled those of C277R homodimers with bi-directional activation but displayed prominent deactivation at subsequent voltage steps to the test potential of −125 mV (Fig. 4*A*). Concatenated C277Y-WT heterodimers exhibited instantaneous current increases followed by deactivation at negative voltage steps. Upon membrane depolarization, we observed very slow activation (Fig. 4*B*). Both heterodimers exhibited bi-directional rectification of instantaneous and late current amplitudes (Fig. 4*C* and *D*).

We employed noise analysis to obtain information about unitary channel properties of heterodimeric

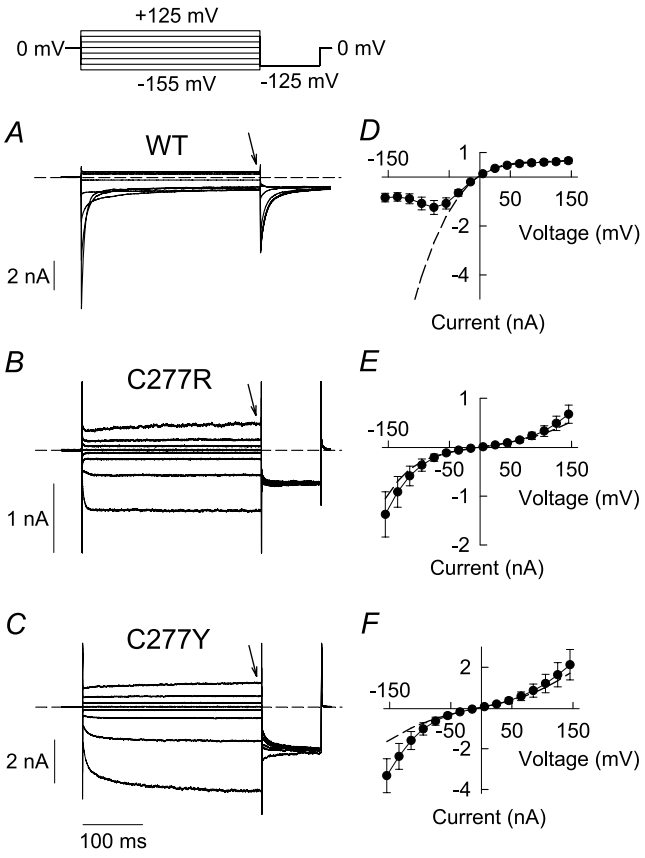

Figure 2. C277R and C277Y modify gating of hClC-1 channels
A–C, pulse protocol and representative current responses of HEK293T cells expressing WT (*A*) or mutant hClC-1 (*B*, C277R; *C*, C277Y). Dashed lines indicate zero current. *D–F*, voltage dependence of instantaneous (dashed lines) and late current amplitudes (symbols) obtained at the end of 300 ms steps to varying potentials (arrows in *A–C*) for WT (*D*, $n = 5$), C277R (*E*, $n = 8$) and C277Y (*F*, $n = 11$) hClC-1.

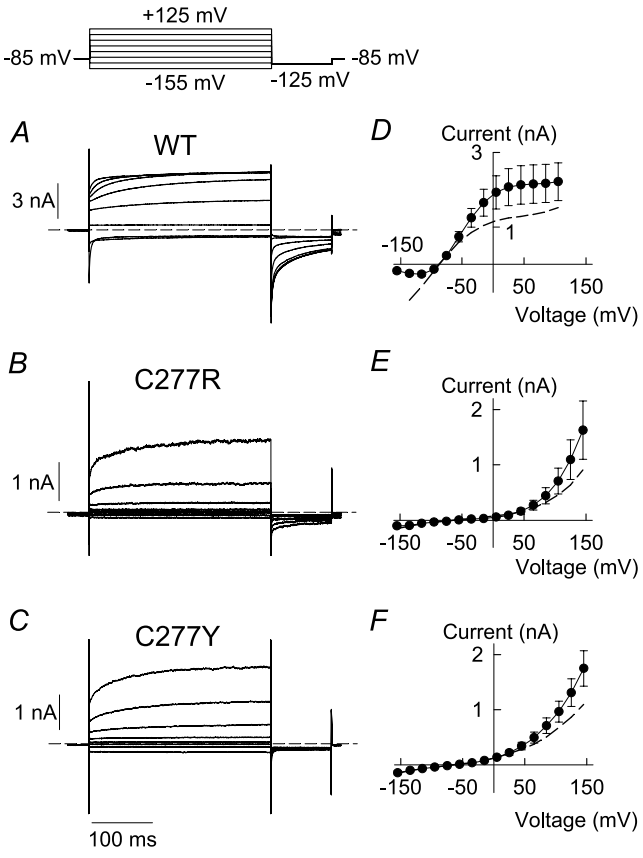

Figure 3. Mutations C277R and C277Y reduce macroscopic chloride conductance at resting membrane potential and physiological internal chloride concentration
A–C, representative current responses of HEK293T cells expressing WT (*A*) or mutant hClC-1 (*B*, C277R; *C*, C277Y) at physiologically low intracellular chloride concentrations (4 mM). Dashed lines indicate zero current. *D–F*, voltage dependence of instantaneous (dashed lines) and late current amplitudes (symbols) (*D*, WT, $n = 8$; *E*, C277R, $n = 4$; *F*, C277Y, $n = 6$).

C277Y-WT channels (Suppl. Fig. 3*A*–*C*). Current amplitudes and variances were determined from short time bins (10 ms) during 2–5 s voltage steps from −5 mV to +105 mV (Suppl. Fig. 3*A*). Plotting variance *versus* current amplitude (Suppl. Fig. 3*B*) gave a linear distribution. Another representation of this relationship is a plot of the ratio of variance by current amplitude changes *versus* the current amplitude. The linear regression of this relationship gives an *x*-axis intercept providing the macroscopic current amplitude one would observe in the case that all channels are fully opened (Alekov & Fahlke, 2009). The absolute open probability at a given time can therefore be calculated as ratio of the current amplitude divided by the *x*-axis intercept. This alternative representation revealed absolute open probabilities that were too low to be accurately determined (Suppl. Fig. 3C). We therefore calculated relative open probabilities by plotting instantaneous tail current amplitudes at a constant test-pulse (−125 mV) *versus* varying pre-pulse potentials (300 ms) and arbitrarily normalized relative open probabilities to 0.25 at +105 mV (Fig. 4*E*). Such normalization overestimates the open probabilities, but allows comparing voltage dependence of gating between heteroconcatamers and WT homodimers. The thus obtained activation curves of both types of concatamer were shifted by more than 100 mV to more depolarizing voltages as compared to WT homodimers (Fig. 4*E*, broken line).

ClC channels are double-barrelled, and heterodimers thus consist of one mutant (C277R or C277Y) protopore and one WT protopore with different gating properties. Since C277R/Y-WT heterodimeric channels exhibit two different protopore gates separation of the distinct individual gating processes is not feasible. However, it is well established that gating of individual protopores in not affected by the adjacent subunit (Ludewig *et al.* 1997). We thus assumed that gating of WT protopores is identical in homodimeric as well as in heterodimeric channels, and that the WT protopore in C277R/Y-WT heterodimeric channels is fully opened by a short voltage step to +180 mV (Accardi & Pusch, 2000). Plotting the instantaneous current amplitude after this short step *versus* the variable conditioning pulse thus provides information about the common gate controlling the WT protopore (Suppl. Fig. 3*D*–*G*). Comparison of such activation curves for WT homodimers and C277R/Y-WT heterodimers thus gives direct insights into C277R/Y-induced changes of the common gate. A plot of the normalized tail current amplitude *versus* the prepulse demonstrates common gating with shifted voltage dependence and decreased minimum open probabilities in heterodimeric channels (Suppl. Fig. 3*E* and *G*). We conclude that open probabilities at resting potential are severely reduced in heterodimeric channels because of altered common gating.

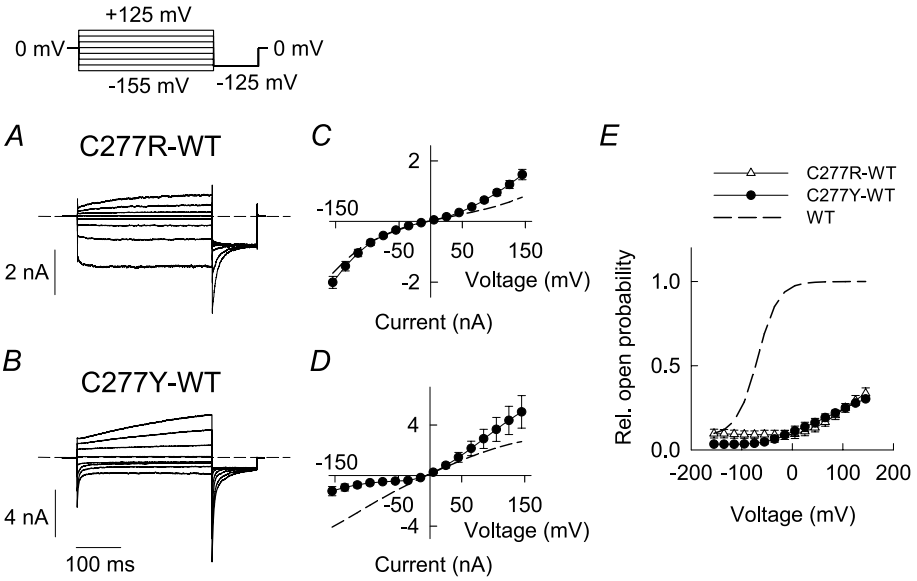

Figure 4. Heterodimeric channels exhibit changed voltage dependence of activation
A and *B*, representative current responses of HEK293T cells expressing concatenated C277R-WT (*A*) or C277Y-WT (*B*) hClC-1 heterodimers. Dashed lines indicate zero current. *C* and *D*, voltage dependence of instantaneous (dashed lines) and late current amplitudes (symbols) (*C*, C277R-WT, $n = 8$; *D*, C277Y-WT, $n = 6$). *E*, voltage dependence of relative open probabilities of concatamers C277R-WT ($n = 12$) and C277Y-WT ($n = 11$). Activation curves are normalized to 0.25 at +105 mV. The dashed line represents the activation curve of WT hClC-1 homodimers.

C277Y modifies protopore and common gating of hClC-1 channels

We next used non-stationary noise analysis to separate the effects of the mutants on protopore and common gating in homodimeric channels. In these experiments, we focused on C277Y hClC-1 because of the more robust expression of this mutant channel. At standard solutions, we obtained seemingly linear current variance *versus* current amplitude relationships (Fig. 5*A* and *B*). However, linear extrapolation of this dependence to zero mean current amplitude would reveal the theoretically impossible negative *y*-axis intercept of approximately $-100\ pA^2$, suggesting a more complex relationship between current variance and amplitude. To further study how the current variance depends on the amplitude, we decreased the external pH (Rychkov *et al.* 1996; Fahlke *et al.* 1996), a manoeuvre that increased C277Y hClC-1 currents at negative potentials (Fig. 5*C*) and resulted in current variance plots that could be used to determine absolute open probabilities of protopore and common gates.

Figure 5*D* shows time dependences of mean current amplitude and variance upon repetitive application of voltage steps from −5 to −155 mV at external pH 5.9. As expected for double-barrelled channels with distinct time and voltage dependences of individual and common gating processes (Fischer *et al.* 2010) the plot of the current variance *versus* the mean current amplitude (Fig. 5*E*) can also not be described by a simple quadratic function that is characteristic for channels with only one single conductance state (Alvarez *et al.* 2002). For those channels, the current variance σ^2 does not only depend on the mean macroscopic current I, the constant number of channels N and the constant protopore current amplitude i, but also

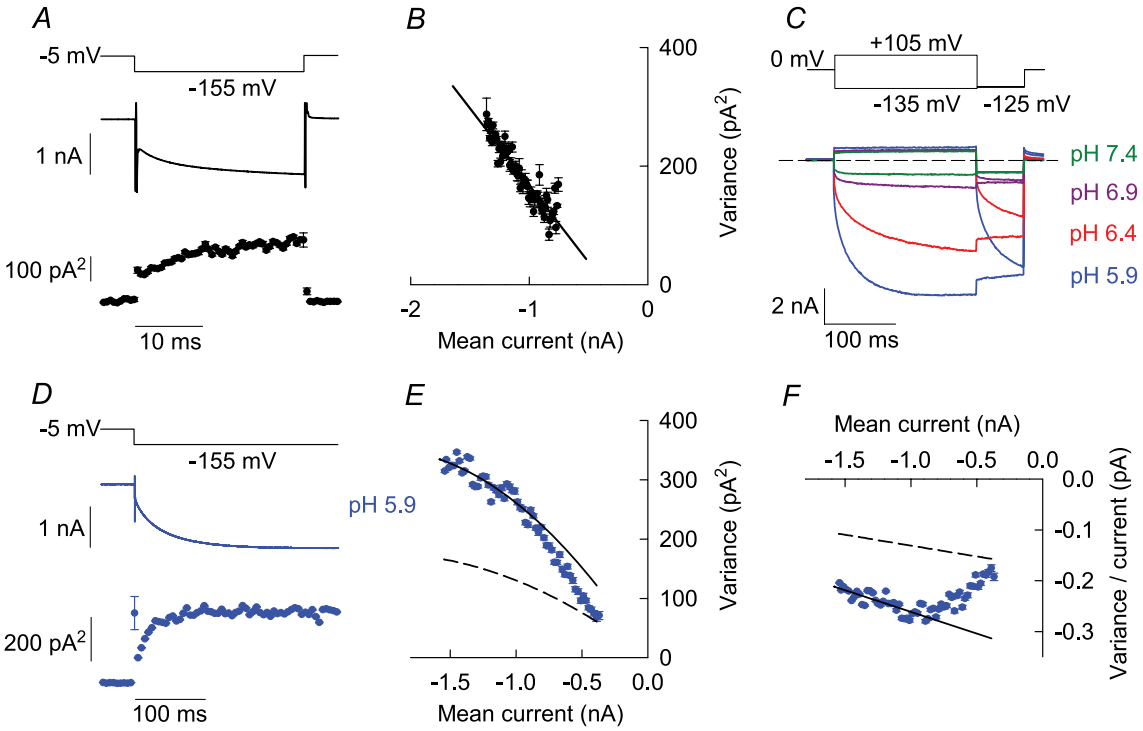

Figure 5. Non-stationary noise analysis allows separation of protopore and common gating of C277Y hClC-1

A, time dependence of the mean current amplitude and variance obtained from repetitive hyperpolarizing voltage steps at extracellular pH 7.4. *B*, current variance and current amplitude appear to be linearly related at pH 7.4 (same data as in *A*). *C*, superposition of current recordings from a single cell at different external pH. The dashed line indicates zero current. *D*, time dependence of mean current amplitude and current variance of a representative recording upon repetitive voltage steps from −5 mV to −155 mV at external pH 5.9. *E*, current variance plotted *versus* mean current amplitude from the data shown in *D*. Lines display predicted current variance relationships for two extreme cases, constitutively open protopore gates (continuous line) or constitutively open common gates (dashed line), respectively. Parabolas were calculated using eqn (3) with $i = -0.17$ pA and $n = 11706$, assuming a steady state open probability of the protopore gate $P_p = 1$. Complete transitions of experimentally determined variances between the parabolas indicate that protopore gate open probabilities increased from nearly closed to almost fully open states. *F*, ratio of variance by current amplitude plotted *versus* mean current amplitude (same data as in *D* and *E*). Variance points at individual sampling times were sorted into evenly spaced current bins and are given as means ± SEM using a bin width of 0.01 nA in *B* and 0.02 nA in *E* and *F*. Mean variances ± SEM in *A* and *D* were calculated from time intervals with a bin width of 0.5 ms in *A* and 5 ms in *D*.

on the time-dependent open probabilities of protopore ($P_p(t)$) and common ($P_c(t)$)gates:

$$\sigma^2 = N \cdot 2i^2 \cdot P_p(t)P_c(t) \cdot (1 - 2P_p(t)P_c(t) + P_p(t)) \quad (1)$$

The macroscopic current is represented by

$$I = N \cdot 2i \cdot P_p(t)P_c(t) \quad (2)$$

Thus, eqn (1) can be converted into

$$\sigma^2 = (1 + P_p(t)) \cdot iI - \frac{1}{N}I^2 \quad (3)$$

Equations (1)–(3) predict a simple quadratic relationship between variance and mean current amplitude for only two specific conditions, i.e. constitutively open protopore gates or constitutively open common gates:

$$\sigma^2 = 2iI - \frac{1}{N}I^2 \quad \text{for } P_p(t) = 1 \quad (4)$$

$$\sigma^2 = iI - \frac{1}{2N}I^2 \quad \text{for } P_c(t) = 1 \quad (5)$$

In the first case, the initial slope of the current variance plot equals twice the protopore current amplitude ($2i$, continuous line in Fig. 5*E*), in the second case only i, the unitary protopore amplitude (dashed line in Fig. 5*E*). These two conditions represent the upper and lower limits of possible variance values for a given number of channels. The experimentally determined C277Y hClC-1 variances are close to the lower parabola for small current amplitudes and approach the upper parabola with increasing amplitude. Equation (3) predicts such a transition upon increases in the open probability of the protopore gate. When the protopore gate reaches its steady state open probability, further changes in variance and current amplitude are exclusively related to changes in common gate open probabilities. The probability of the channel to be open can be estimated when considering that the maximum of the parabola corresponds to 50% of channels being open (Alvarez *et al.* 2002). Therefore, the total open probability of the C277Y channels is far below 50%, resulting from low open probability of the common gate, even though the steady state open probability of the protopore gates is high.

Figure 5*F* shows the ratio of the variance by the mean current amplitude plotted *versus* the mean current amplitude.

$$\frac{\sigma^2}{I} = (1 + P_p(t)) \cdot i - \frac{1}{N}I \quad (6)$$

Straight lines in Fig. 5*F* represent the same extremes that have been plotted as parabolas in Fig. 5*E*. After the protopore gate open probability has reached steady state conditions, eqn (6) predicts a linear dependence with the slope of $-1/N$. Thus, a linear fit to the data points with current amplitudes below −1 nA allowed determination of the number of channels.

Unfortunately, this analysis does not allow separate determination of absolute open probabilities of individual and common gates. However, it permits exclusion of steady state open probability P_p values that are lower than 0.75 (Suppl. Fig. 4). For this consideration, we assumed different steady state protopore gate open probabilities P_p and calculated the resulting unitary protopore current amplitude i. For each i value we then constructed variance *versus* current relationships for two extreme cases, constitutively open protopore gates (continuous lines in Suppl. Fig. 4) or constitutively open common gates (dashed lines in Suppl. Fig. 4). As discussed above, the current variance at a given current amplitude cannot be lower than the value predicted for constitutively open common gates. We found that steady state protopore gate open probabilities below 0.75 were incompatible with initial variance values obtained immediately after the voltage step (Suppl. Fig. 4). We thus simply calculated unitary current amplitudes and absolute open probabilities for the two limiting values of the protopore gate open probability $P_p = 0.75$ and $P_p = 1$. Assuming that the steady state open probability of the protopore gate is 1, the y-axis intercept of the linear regression line corresponds to twice the protopore unitary current amplitude and the x-axis intercept is $I = 2iN$, representing the maximum current amplitude of the channel in the case that the channel is fully opened and the product of protopore and common gate open probabilities is 1. We calculated mean protopore current amplitude i to be -0.17 ± 0.01 pA and an absolute steady state open probability of 0.28 ± 0.03 at –155 mV and pH 5.9 ($n = 5$). This steady state open probability equals the open probability of the common gate, if steady state P_p is 1. For P_p of 0.75, our analysis provided a unitary protopore current amplitude of -0.20 ± 0.01 pA, an absolute open probability of the common gate of 0.33 ± 0.03 and a steady state probability of both gates (and thus the ion conduction pathway) being open of 0.25 ± 0.02 ($n = 5$), all values again at external pH 5.9. The unitary current amplitude calculated for the protopore gate open probability P_p of 1 is exactly the amplitude we observed in single channel recordings (see below, Fig. 8). We therefore assumed steady-state P_p being 1 at −155 mV and pH 5.9 for all further calculations.

Figure 6 shows noise analyses from a representative cell that was consecutively perfused with solutions of different external pH. We applied short voltage steps (25 ms) from −5 to −155 mV and determined mean current amplitudes

and variances for pH 7.4, 6.9, 6.4 and 5.9. Variance values and variance/current were plotted *versus* mean current amplitudes in Fig. 6*A* and *B*. These plots are in full agreement with the notion that unitary protopore current amplitudes were identical for each tested pH ($n = 6$). Since protopore gating is responsible for the shift of variance values between i and $2i$ parabola (eqn (3) and Suppl. Fig. 4), the almost complete transitions between the extremes indicate that protopore gate open probabilities increased from nearly closed to fully open states only at low pH (Fig. 6*A* and *B*). With pH 6.9 and 7.4, however, the transition is incomplete indicating that protopore gates did not fully open at neutral pH. Nevertheless, low common gate open probabilities appear to be the main limiting factor of the total open probability.

We next determined the voltage dependence of relative open probabilities by plotting instantaneous tail current amplitudes at −125 mV *versus* varying pre-pulse potentials (using pulse protocols as shown in Fig. 2) and normalized these values to the absolute open probability obtained from non-stationary noise analysis at −155 mV and pH 5.9 (Fig. 6*C*). With increasing pH activation curves shifted to the left towards more negative potentials, resulting in absolute open probabilities below 0.03 over the entire voltage range at neutral pH.

Single channel recordings of WT and C277Y hClC-1 channels

To confirm the results of noise analysis at the single channel level we next performed unitary current measurements from excised inside-out patches. Figure 7 shows representative single channel recordings from WT and mutant C277Y hClC-1 channels obtained at −100 mV. We chose an external pH of 6.4 to increase open probability of mutant and WT channels (Saviane *et al.* 1999). For WT as well as for mutant channels we observed two equally spaced conductance states that correspond to opening of only one of the two protopores (open1) and joint openings of both protopores (open2) of the dimeric channel. Current transitions between closed and open2 states indicate opening and closure of the common gate when both protopore gates are open, as depicted in the sections with expanded time scales for WT (Fig. 7*A* section *a*) and for mutant C277Y channels (Fig. 7*B* section *b*). Whereas WT channels displayed higher levels of activity with some short interruptions through closure of the common gate, mutant channels displayed rare openings. The rare frequency of openings precluded an accurate determination of the number of mutant channels in a patch and prevented more detailed investigations of open probabilities from single channel recordings.

Unitary protopore current amplitudes were determined by fitting amplitude histograms with a sum of three Gaussian functions (Fig. 7*C*). Mean protopore current amplitude obtained at −100 mV was significantly larger for WT hClC-1 than for mutant channels (Fig. 7*D*; WT: -0.13 ± 0.01 pA, $n = 5$; C277Y: -0.09 ± 0.003 pA, $n = 7$). Since single channel current amplitudes can only be measured at a restricted voltage range, we extrapolated measured unitary current amplitudes at −100 mV to calculate unitary currents for various voltages using instantaneous current–voltage relationship from whole cell recordings (Fig. 8*A*; pH 7.4). We thus obtained unitary protopore current amplitude of −0.18 pA at −155 mV for C277Y channels and −0.27 pA for WT channels, in very good agreement to our results from noise analyses (C277Y: -0.17 ± 0.01 pA, $n = 5$; WT: 0.29 ± 0.01 pA, $n = 3$; WT values were calculated using eqn (3) with a steady state open probability of 0.20 ± 0.02 for the protopore gate).

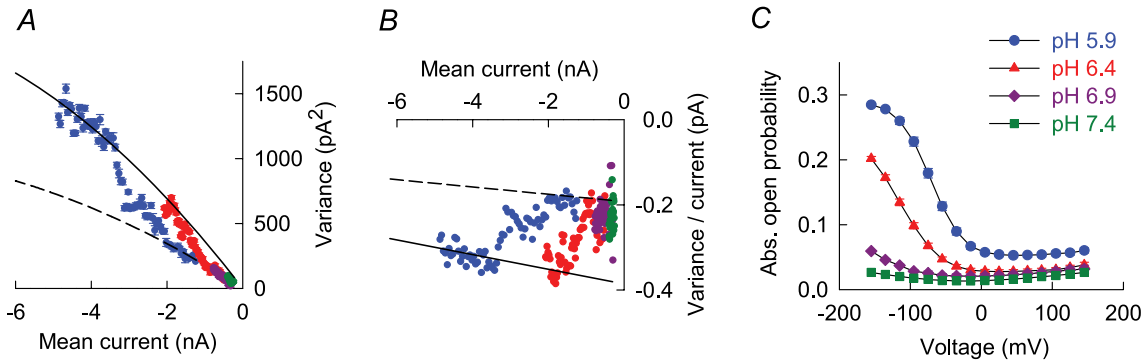

Figure 6. Non-stationary noise analysis predicts low absolute open probability of C277Y hClC-1
Current variance (*A*) and ratio of variance by current amplitude (*B*) plotted *versus* mean current amplitude of a single cell investigated under varying external pH. Protopore unitary currents are identical for each pH. *C*, voltage dependence of absolute open probabilities at different pH (pH 7.4, $n = 17$; pH 6.9, $n = 6$; pH 6.4, $n = 10$; pH 5.9, $n = 11$). Activation curves illustrate very low absolute open probabilities of C277Y hClC-1 at pH 7.4.

C277Y-induced changes in unitary current amplitude and absolute open probabilities predict dramatic reduction of muscle chloride conductance

Figure 8*B* shows the voltage dependence of absolute open probabilities for C277Y and WT hClC-1 as obtained from noise analysis at physiological pH. Figure 8*C* combines protopore current amplitudes and open probabilities and displays the voltage dependence of the mean steady-state protopore current amplitude of mutant and WT channels. This comparison allows prediction of the decrease in macroscopic chloride conductance in mutant muscle fibres of homozygous patients assuming identical expression and surface insertion. C277Y results in a reduction of chloride current amplitudes to 3.6% of WT current amplitude at resting membrane potential (−85 mV).

C277Y modifies pore properties of hClC-1 channels

Reduced unitary current amplitudes indicate that C277Y not only alters gating but also the conduction properties of hClC-1. As an additional functional parameter of the ion conduction pathway, we investigated the ability of C277Y hClC-1 to select between anions. Figure 9*A* displays representative current recordings of C277Y hClC-1 channels from cells internally dialysed with a pipette solution containing 4 mM Cl^- and 120 mM Br^-, NO_3^- or I^-, respectively, and a standard external solution. Figure 9*B*

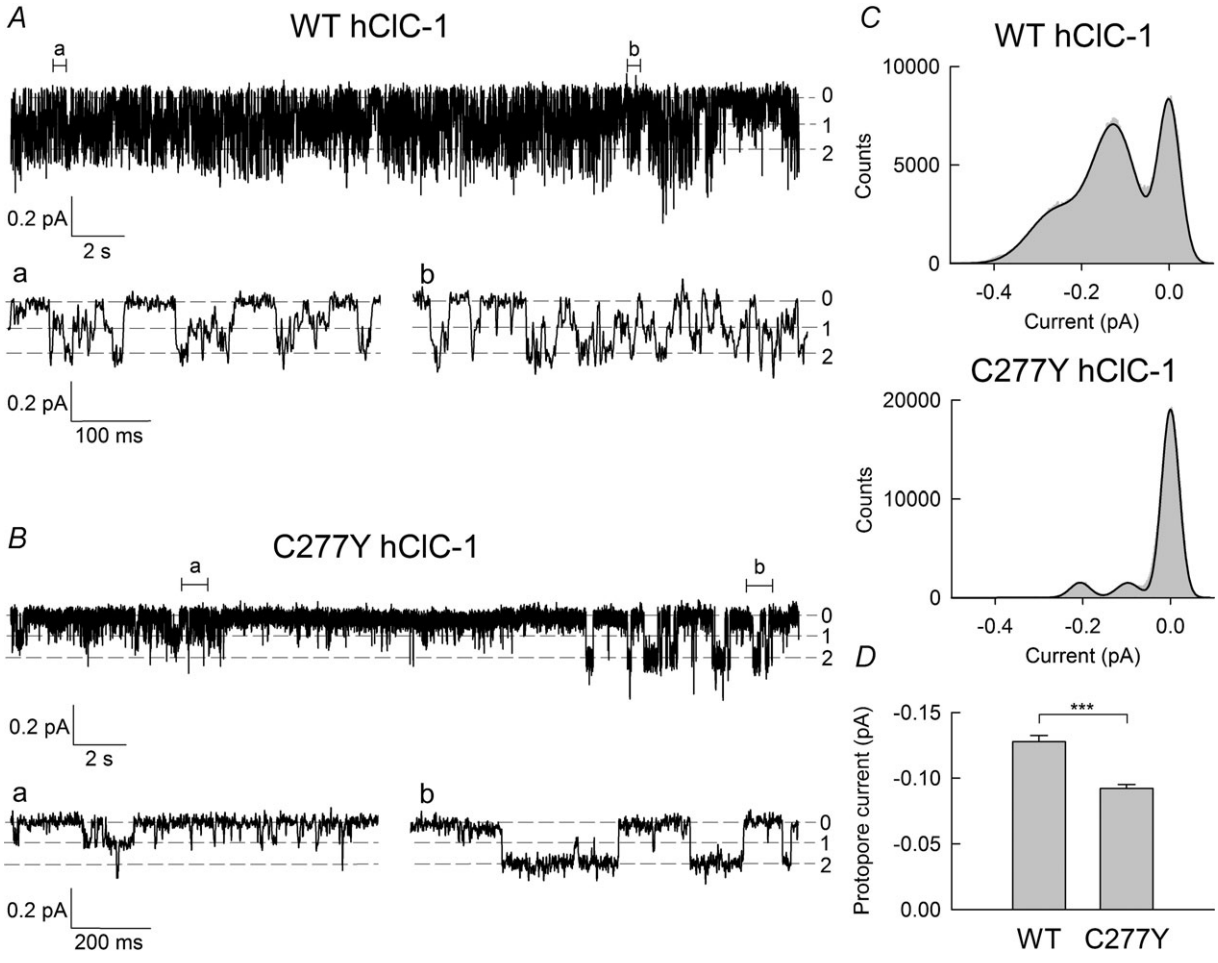

Figure 7 Single channel recordings of WT and mutant C277Y hClC-1
Representative recordings of single WT (*A*) and mutant C277Y hClC-1 channels (*B*) from excised inside-out patches at −100 mV, internal pH 7.4 (bath solution) and external pH 6.4 (pipette solution). Segments of the recordings that are shown on an expanded time scale are indicated as (a) and (b). *C*, amplitude histograms were obtained from complete traces shown in *A* and *B*. Black lines represent fits with a sum of three Gaussian distributions. Unitary protopore open probabilities were calculated from the areas under the Gaussian fits providing values of 0.47 for WT and 0.12 for C277Y hClC-1. *D*, mean protopore amplitudes at −100 mV were significantly lower for mutant C277Y channels ($n = 7$) than for WT channels ($n = 5$) (***Student's *t* test with $P < 0.0001$).

shows the corresponding current–voltage relationships. We chose modification of internal anions since larger and polyatomic anions would reduce the anion conductance around the reversal potential when applied externally (Fahlke *et al.* 1997*b*). Internal variation of anion thus renders measurements of reversal potentials less sensitive to changes in leak resistances than external solution exchange.

Reversal potentials determined on cells internally dialysed with various anions were positive ($V_{rev,Br} = +7.9 \pm 0.3$ nA ($n = 6$); $V_{rev,NO3} = +23.9 \pm 1.2$ nA ($n = 9$); $V_{rev,I} = +24.6 \pm 0.9$ nA ($n = 6$)), in contrast to corresponding measurements with WT that resulted in negative reversal potentials (Fahlke *et al.* 1997*b*). Measured reversal potentials were independent of expression levels, demonstrating that our measurements were not affected by endogenous currents (Fig. 9*C*). We used these results to calculate relative permeabilities P_X/P_{Cl} using the Goldmann–Hodgkin–Katz equation. C277Y inverts the anion permeability sequence of hClC-1 to $I^- = NO_3^- > Br^- > Cl^-$ as compared to $Cl^- > Br^- > NO_3^- > I^-$ for WT channels (Fig. 9*D*).

Discussion

Myotonia congenita was one of the first genetic diseases shown to be caused by mutations in genes encoding ion channels (Koch *et al.* 1992; George *et al.* 1993). In recent years, a large number of mutations have been identified in the *CLCN1* gene encoding the muscle chloride channel hClC-1. These mutations are dispersed throughout the whole coding region and result in distinct alterations of channel function. Such random sequence alterations that are known to impair channel function permit unexpected insights into structure–function relationship and thus provide an alternative approach to identify sequence determinants of channel functions. In ClC-5, another member of the ClC channel/transporter family, a large number of naturally occurring mutations associated with Dent's disease are located in the interface region of the homodimer and induce misfolding and early degradation of the protein (Lourdel *et al.* 2012). In contrast, mutations that impair protein function and do not interfere with protein trafficking and stability are localized in close proximity to the conduction pathway. We studied here two naturally occurring mutations of ClC-1 channels that predict substitutions of cysteine 277 at the end of the G helix, a position that interconnects the interface region with the conduction pathway (Fig. 1*B*). This residue is homologous to cysteine 212 in ClC-0 that was shown to be a key determinant of slow common gating of this channel (Lin *et al.* 1999). C212S ClC-0 is characterized by the complete absence of common gating and subsequent work demonstrated that neutralizing the corresponding cysteine 277 in hClC-1 (Accardi *et al.* 2001) or cysteine 256 in ClC-2 (Zuniga *et al.* 2004; de Santiago *et al.* 2005) also affected slow gating of these channels. However, another ClC-type anion channel, rat ClC-K1, has a threonine instead of cysteine at this position, but exhibits slow common gating (Fischer *et al.* 2010), demonstrating that a cysteine at this amino acid position is not crucial for this particular gating process in all ClC channels.

C277R as well as C277Y cause a dramatic reduction of macroscopic currents in cells expressing hClC-1 homodimers (Fig. 2). This finding predicts a significant reduction of muscle chloride conductance in homozygous patients. Using noise analysis we studied one of the two mutations, C277Y, in more detail, and found that it dramatically reduces the absolute open probability of homodimeric channels to 0.02 at −85 mV compared to 0.38 in WT channels (Fig. 8*B*). Such low open probabilities were also determined for heterodimers consisting of one WT and one C277R/Y hClC-1 protopore (Fig. 4). We also

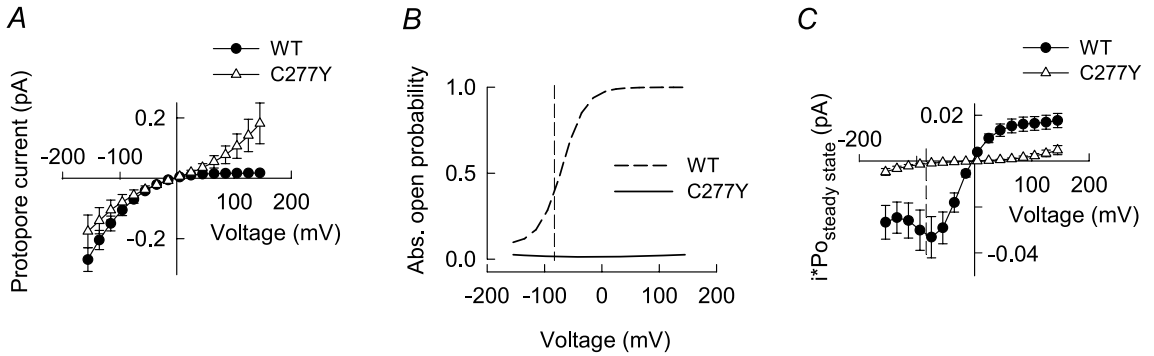

Figure 8. C277Y-induced changes in absolute open probabilities and unitary current amplitudes predict dramatically reduced chloride conductances in myotonic muscle fibres
A, voltage dependences of instantaneous current amplitudes (same data as in Fig. 2*D* and *F*), normalized to unitary protopore current amplitudes obtained from single channel recordings at −100 mV (Fig. 7*D*). *B*, voltage dependences of absolute open probabilities of WT and C277Y hClC-1 at physiological pH. *C*, comparison of WT and C277Y steady-state current amplitudes displayed as mean current amplitude per single protopore.

recorded macroscopic currents from cells transfected with identical amounts of WT and mutant (C277R or C277Y) hClC-1. Since the tested mutations do not affect expression levels of hClC-1 (Suppl. Fig. 1), one might expect that 50% of all channels would be heterodimers carrying one mutant and one WT allele in these cells. However, the efficiency of forming heterodimers appears to be different between the two mutations. For C277R, we observed currents that resemble WT homodimers. This finding is in full agreement with the notion that C277R homo- and heterodimers exhibit very low open probabilities and that WT homodimers consequently dominate the macroscopic currents. However, cells expressing equal amounts of WT and C277Y hClC-1 exhibit currents that are very similar to currents conducted by heterodimers. This finding could be due to an improved heterodimerization of WT and C277Y subunits, i.e. that WT has a higher likelihood of associating with C277Y hClC-1. Since we are unable to quantify the ability to form heterodimers, we cannot predict macroscopic chloride conductances in muscle fibres of heterozygous patients.

In the five investigated families the patients' parents did not suffer from myotonia, thus strongly supporting a recessive inheritance mode of C277R and C277Y. Such recessive inheritance might be explained by incomplete expression of these particular mutations with a mild additional effect of accompanying mutations in compound heterozygous patients. The F167L mutation found in patients 1, 2 and 3 together with C277R has been shown to mildly affect hClC-1 properties, shifting the activation curve by about 14 mV to more positive potentials (Zhang *et al.* 2000). I527T that was also identified in patient 5 shifted the midpoint of activation of homodimers from -72.1 ± 4.2 mV for WT channels ($n = 6$) to -46.3 ± 1.6 mV for I527T hClC-1 ($n = 5$) due to altered voltage dependence of slow common gating (Suppl. Fig. 5). Fast protopore gating remained unaffected even though the minimum open probability

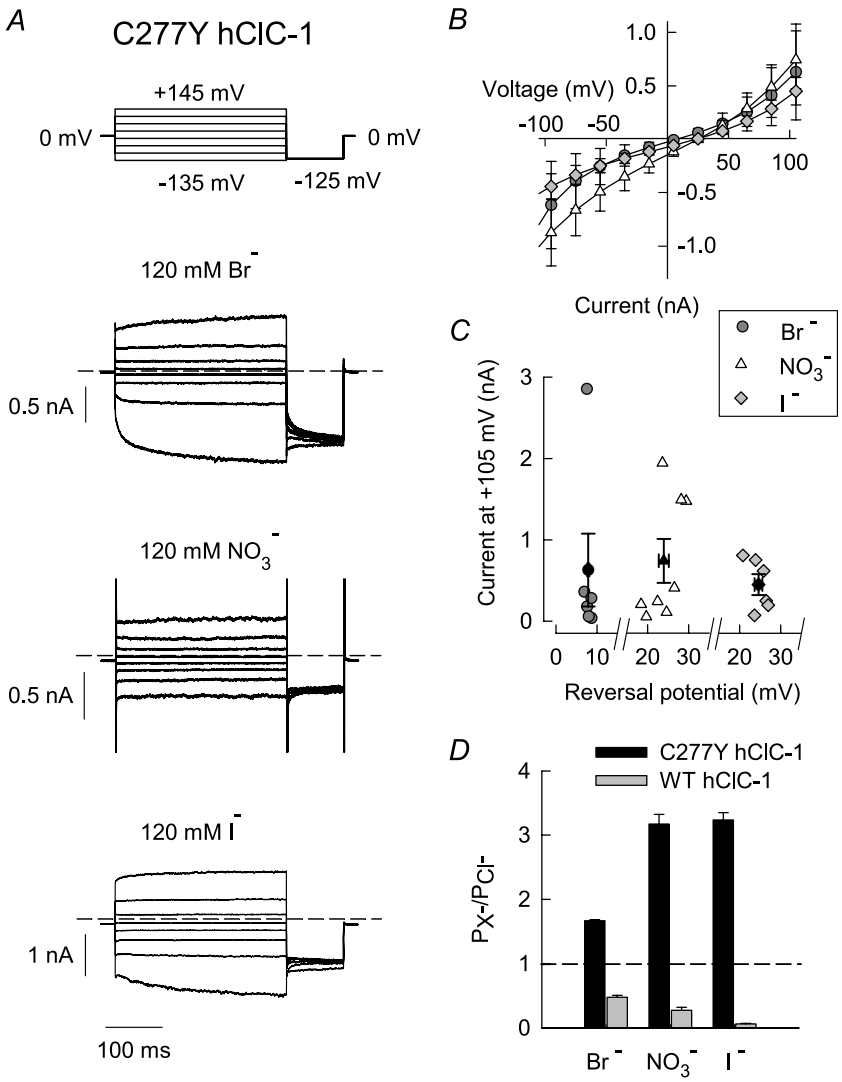

Figure 9. C277Y modifies pore properties of hClC-1 channels
A, representative current recordings from cells internally dialysed with a pipette solution containing 4 mM Cl^- and 120 mM Br^-, NO_3^- or I^-. Dashed lines indicate zero current. *B*, voltage dependence of current amplitudes obtained from cells internally dialysed with Br^- ($n = 6$), NO_3^- ($n = 8$) or I^- ($n = 6$). *C*, current amplitudes of different cells at +105 mV plotted *versus* their reversal potentials demonstrate that reversal potentials were independent from expression levels in transfected cells. The plot includes individual values (open and grey filled symbols) and the mean values ± SEM (black filled symbols: Br^-, $n = 6$; NO_3^-, $n = 8$; I^-, $n = 6$). *D*, mutation C277Y (black bars: Br^-, $n = 6$; NO_3^-, $n = 9$; I^-, $n = 6$) altered permeability sequence to $I^- = NO_3^- > Br^- > Cl^-$ as compared to $Cl^- > Br^- > NO_3^- > I^-$ for WT channels (grey bars: Br^-, $n = 6$; NO_3^-, $n = 6$; I^-, $n = 4$).

of the protopore gates was slightly increased. Accordingly, modification of gating by mutations F167L and I257T suggests that resting chloride conductance is even lower in muscle of compound heterozygous patients than in heterozygous patients carrying C277R/Y mutations on one allele and WT on the other, which contributes to disease expression. Our functional data together with existing genetic information might be explained by preferential expression or advanced stability of F167L or I257T homodimers in comparison to C277R/Y homodimers and heterodimeric channels in the compound heterozygous patients.

We combined noise analysis and single channel recordings to define the alterations of unitary channel properties of mutant channels. Noise analyses on double-barrelled channels are complicated by the occurrence of two different conductance states. For such channels, fitting a simple quadratic function to the variance values plotted *versus* mean current provides apparent unitary channel amplitudes that are intermediate between single (i) and double ($2i$) protopores. We therefore used a modified approach that takes the influence of time-dependent protopore gating into account. Both, single channel recordings and noise analysis revealed C277Y protopore currents reduced to 72% of WT protopore currents at −100 mV and less than two-thirds of WT unitary currents at −155 mV. The altered selectivity among anions (Fig. 9) is further support for alterations of the ion conduction pathway of hClC-1 by C277Y. C277Y hClC-1 exhibits larger permeabilities for Br^-, I^- and NO_3^- than for Cl^- and thus an inverted permeability sequence as compared to WT hClC-1.

C277 does not directly contribute to the ion conduction pathway of ClC isoforms as deduced from the existing three-dimensional structures (Dutzler *et al.* 2002, Dutzler *et al.* 2003; Feng *et al.* 2010). However, the side chain of this amino acid might interact with the F helix harbouring the gating glutamate, E232, and a neighbouring K231. K231 has been shown to be a crucial determinant of anion selectivity of hClC-1. Charge neutralizing or inverting mutations at position 231 invert the selectivity sequence of hClC-1, and adding a small cationic adduct by reacting MTSEA to Cys 231 restores WT selectivity (Fahlke *et al.* 1997*d*). Moreover, changes in charge and length of the side chain at position 165 modify unitary current amplitudes of ClC-0 (Lin & Chen, 2000). These findings suggest that anions might come in close proximity to the side chain of K231 in hClC-1. Alterations of the position of this lysine might thus explain altered pore properties of C277Y, and changes in the position of E232 provide a structural explanation for the modified gating properties.

Gating processes that mediate the cooperative opening and closing of both protopores of double-barrelled ClC channels were crucial for identifying the unique architecture of this class of ion channels (Miller, 1982). Furthermore, they illustrate a possible physiological importance of association of multiple ion conduction pathways in a single channel. However, little is known about the mechanism underlying these processes. Cysteine 277 was the first residues whose exchange to serine had pronounced effects on common gating but not on protopore gating of hClC-1 (Accardi *et al.* 2001). Analysing naturally occurring Cys-to-Arg and Cys-to-Tyr disease-causing mutations at this position, we show here that mutations in C277 do not only modify common gating, but also unitary current amplitudes, anion selectivity as well as protopore gating.

Skeletal muscle fibres are unique among excitable tissue in a large resting chloride conductance. The here reported reduction in the open probability of C277R/Y hClC-1 at resting membrane potential together with additional alterations of conduction properties predicts a significant reduction of the resting chloride conductance, an increase of the length constants of the sarcolemma and the autonomous generation of action potentials in myotonic fibres (Adrian & Bryant, 1974).

References

Accardi A, Ferrera L & Pusch M (2001). Drastic reduction of the slow gate of human muscle chloride channel (CLC-1) by mutation C277S. *J Physiol* **534**, 745–752.

Accardi A & Pusch M (2000). Fast and slow gating relaxations in the muscle chloride channel CLC-1. *J Gen Physiol* **116**, 433–444.

Adrian RH & Bryant SH (1974). On the repetitive discharge in myotonic muscle fibres. *J Physiol* **240**, 505–515.

Alekov A & Fahlke Ch (2009). Channel-like slippage modes in the human anion/proton exchanger ClC-4. *J Gen Physiol* **133**, 485–496.

Alvarez O, Gonzalez C & Latorre R (2002). Counting channels: a tutorial guide on ion channel fluctuation analysis. *Adv Physiol Educ* **26**, 327–341.

Barry PH (1994). JPCalc, a software package for calculating liquid junction potential corrections in patch-clamp, intracellular, epithelial and bilayer measurements and for correcting junction potential measurements. *J Neurosci Methods* **51**, 107–116.

Bernard G, Poulin C, Puymirat J, Sternberg D & Shevell M (2008). Dosage effect of a dominant *CLCN1* mutation: a novel syndrome. *J Child Neurol* **23**, 163–166.

Cederholm JM, Rychkov GY, Bagley CJ & Bretag AH (2010). Inter-subunit communication and fast gate integrity are important for common gating in hClC-1. *Int J Biochem Cell Biol* **42**, 1182–1188.

de Santiago JA, Nehrke K & Arreola J (2005). Quantitative analysis of the voltage-dependent gating of mouse parotid ClC-2 chloride channel. *J Gen Physiol* **126**, 591–603.

Duffield M, Rychkov GY, Bretag AH & Roberts ML (2003). Involvement of helices at the dimer interface in ClC-1 common gating. *J Gen Physiol* **121**, 149–161.

Dutzler R, Campbell ED, Cadene M, Chait MB & MacKinnon R (2002). X-ray structure of a ClC chloride channel at 3.0 A reveals the molecular basis of anion selectivity. *Nature* **415**, 287–294.

Dutzler R, Campbell ED & MacKinnon R (2003). Gating the selectivity filter in ClC chloride channels. *Science* **300**, 108–112.

Fahlke C, Beck CL & George AL Jr (1997*a*). A mutation in autosomal dominant myotonia congenita affects pore properties of the muscle chloride channel. *Proc Natl Acad Sci U S A* **94**, 2729–2734.

Fahlke C, Dürr C & George AL Jr (1997*b*). Mechanism of ion permeation in skeletal muscle chloride channels. *J Gen Physiol* **110**, 551–564.

Fahlke C, Knittle TJ, Gurnett CA, Campbell KP & George AL Jr (1997*c*). Subunit stoichiometry of human muscle chloride channels. *J Gen Physiol* **109**, 93–104.

Fahlke C, Rosenbohm A, Mitrovic N, George AL Jr & Rüdel R (1996). Mechanism of voltage-dependent gating in skeletal muscle chloride channels. *Biophys J* **71**, 695–706.

Fahlke C, Rüdel R, Mitrovic N, Zhou M & George AL Jr (1995). An aspartic acid residue important for voltage-dependent gating of human muscle chloride channels. *Neuron* **15**, 463–472.

Fahlke C, Yu HT, Beck CL, Rhodes TH & George AL Jr (1997*d*). Pore-forming segments in voltage-gated chloride channels. *Nature* **390**, 529–532.

Feng L, Campbell EB, Hsiung Y & MacKinnon R (2010). Structure of a eukaryotic CLC transporter defines an intermediate state in the transport cycle. *Science* **330**, 635–641.

Fischer M, Janssen AG & Fahlke C (2010). Barttin activates ClC-K channel function by modulating gating. *J Am Soc Nephrol* **21**, 1281–1289.

Fournier E, Viala K, Gervais H, Sternberg D, Arzel-Hézode M, Laforet P, Eymard B, Tabti N, Willer JC, Vial C & Fontaine B (2006). Cold extends electromyography distinction between ion channel mutations causing myotonia. *Ann Neurol* **60**, 356–365.

George AL, Crackower MA, Abdalla JA, Hudson AJ & Ebers GC (1993). Molecular basis of Thomsen's disease (autosomal dominant myotonia congenita). *Nature Genet* **3**, 305–310.

Hebeisen S, Biela A, Giese B, Muller-Newen G, Hidalgo P & Fahlke C (2004). The role of the carboxyl terminus in ClC chloride channel function. *J Biol Chem* **279**, 1340–1347.

Hebeisen S, Heidtmann L, Cosmelli D, Gonzalez C, Poser B, Latorre R, Alvarez O & Fahlke C (2003). Anion permeation in human ClC-4 channels. *Biophys J* **84**, 2306–2318.

Hebeisen S & Fahlke C (2005). Carboxy-terminal truncations modify the outer pore vestibule of muscle chloride channels. *Biophys J* **89**, 1710–1720.

Heinemann SH & Conti F (1992). Nonstationary noise analysis and application to patch clamp recordings. *Methods Enzymol* **207**, 131–148.

Jentsch TJ (2008). CLC chloride channels and transporters: from genes to protein structure, pathology and physiology. *Crit Rev Biochem Mol Biol* **43**, 3–36.

Koch MC, Steinmeyer K, Lorenz C, Ricker K, Wolf F, Otto M, Zoll B, Lehmann-Horn F, Grzeschik KH, & Jentsch TJ (1992). The skeletal muscle chloride channel in dominant and recessive human myotonia. *Science* **257**, 797–800.

Lehmann-Horn F, Mailander V, Heine R & George AL Jr (1995). Myotonia levior is a chloride channel disorder. *Hum Mol Genet* **4**, 1397–1402.

Lehmann-Horn F, Orth M, Kuhn M & Jurkat-Rott K (2011). A novel N440K sodium channel mutation causes myotonia with exercise-induced weakness – exclusion of *CLCN1* exon deletion/duplication by MLPA. *Acta Myologica* **30**, 133–137.

Lin CW & Chen TY (2000). Cysteine modification of a putative pore residue in ClC-0: implication for the pore stoichiometry of ClC chloride channels. *J Gen Physiol* **116**, 535–546.

Lin YW, Lin CW & Chen TY (1999). Elimination of the slow gating of ClC-0 chloride channel by a point mutation. *J Gen Physiol* **114**, 1–12.

Lourdel S, Grand T, Burgos J, González W, Sepúlveda FV & Teulon J (2012). ClC-5 mutations associated with Dent's disease: a major role of the dimer interface. *Pflugers Arch* **463**, 247–256.

Ludewig U, Pusch M & Jentsch TJ (1997). Independent gating of single pores in CLC-0 chloride channels. *Biophys J* **73**, 789–797.

Miller C (1982). Open-state substructure of single chloride channels from *Torpedo* electroplax. *Philos Trans R Soc Lond B Biol Sci* **299**, 401–411.

Rychkov GY, Pusch M, Astill DSJ, Roberts ML, Jentsch TJ & Bretag AH (1996). Concentration and pH dependence of skeletal muscle chloride channel ClC-1. *J Physiol* **497**, 423–435.

Saviane C, Conti F & Pusch M (1999). The muscle chloride channel ClC-1 has a double-barreled appearance that is differentially affected in dominant and recessive myotonia. *J Gen Physiol* **113**, 457–468.

Weinberger S, Sternberg D, Lehmann-Horn F, Fahlke C & Fischer M (2011). Mutations C277Y and C277R cause dysfunction of human ClC-1 chloride channels resulting in myotonia congenita. *Acta Physiol* 201, 292.

Wollnik B, Kubisch C, Steinmeyer K & Pusch M (1997). Identification of functionally important regions of the muscular chloride channel CIC-1 by analysis of recessive and dominant myotonic mutations. *Hum Mol Genet* **6**, 805–811.

Wu FF, Ryan A, Devaney JM, Warnstedt M, Korade-Mirnics Z, Poser B, Escriva MJ, Pegoraro E, Yee AS, Felice KJ, Giuliani MJ, Mayer RF, Mongini T, Palmucci LM, Marino M, Rüdel R, Hoffman EP & Fahlke C (2002). Novel *CLCN1* mutations with unique clinical and electrophysiological consequences. *Brain* **125**, 2392–2407.

Zhang J, Sanguinetti MC, Kwiecinski H & Ptacek LJ (2000). Mechanism of inverted activation of ClC-1 channels caused by a novel myotonia congenita mutation. *J Biol Chem* **275**, 2999–3005.

Zuniga L, Niemeyer MI, Varela D, Catalan M, Cid LP & Sepulveda FV (2004). The voltage-dependent ClC-2 chloride channel has a dual gating mechanism. *J Physiol* **555**, 671–682.

Author contributions

Ch.F. and M.F. conceived and designed the experiments. D.S., F.L.-H. and K.J.-R. obtained clinical data from the myotonic patients and performed molecular genetics diagnosis at Hôpital Pitié-Salpêtrière, Paris, and University of Ulm. Mutagenesis and expression studies were performed by D.W., T.B. and B.B. Electrophysiological experiments were performed and analysed by S.W. and M.F. at Medizinische Hochschule Hannover. Ch.F. and M.F. drafted and revised the manuscript with input from the co-authors. All authors approved the final version of the manuscript.

Acknowledgements

We thank Drs Alexi Alekov, Raul Guzman Castro, Peter Kovermann and Gabriel Stölting for helpful discussions and Petra Kilian for excellent technical assistance. These studies were supported by the Muscular Dystrophy Association (MDA 91492 to Ch.F.).